Supporting Information for

Surface Patterning of Metal Zinc Electrode with an In-Region Zincophilic Interface for High-Rate and Long-Cycle-Life Zinc Metal Anode

Tian Wang[1], Qiao Xi[2], Kai Yao[3], Yuhang Liu[2], Hao Fu[4], Venkata Siva Kavarthapu[1], Jun Kyu Lee[1], Shaocong Tang[1], Dina Fattakhova-Rohlfing[3], Wei Ai[2,]*, Jae Su Yu[1,]*

[1] Department of Electronics and Information Convergence Engineering, Institute for Wearable Convergence Electronics, Kyung Hee University, Yongin-si, Gyeonggi-do 17104, Republic of Korea

[2] Frontiers Science Center for Flexible Electronics (FSCFE) & Shaanxi Institute of Flexible Electronics (SIFE), Northwestern Polytechnical University (NPU), 127 West Youyi Road, Xi'an 710072, People's Republic of China

[3] Institute of Energy and Climate Research, Materials Synthesis and Processing, Forschungszentrum Jülich GmbH, 52425 Jülich, Germany

[4] School of Chemical Engineering, Sungkyunkwan University, 2066 Seobu-ro, Jangan-gu, Suwon-si, Gyeonggi-do, Republic of Korea

*Corresponding authors. E-mail: iamwai@nwpu.edu.cn (W. Ai), jsyu@khu.ac.kr (J. S. Yu)

Supplementary Figures and Table

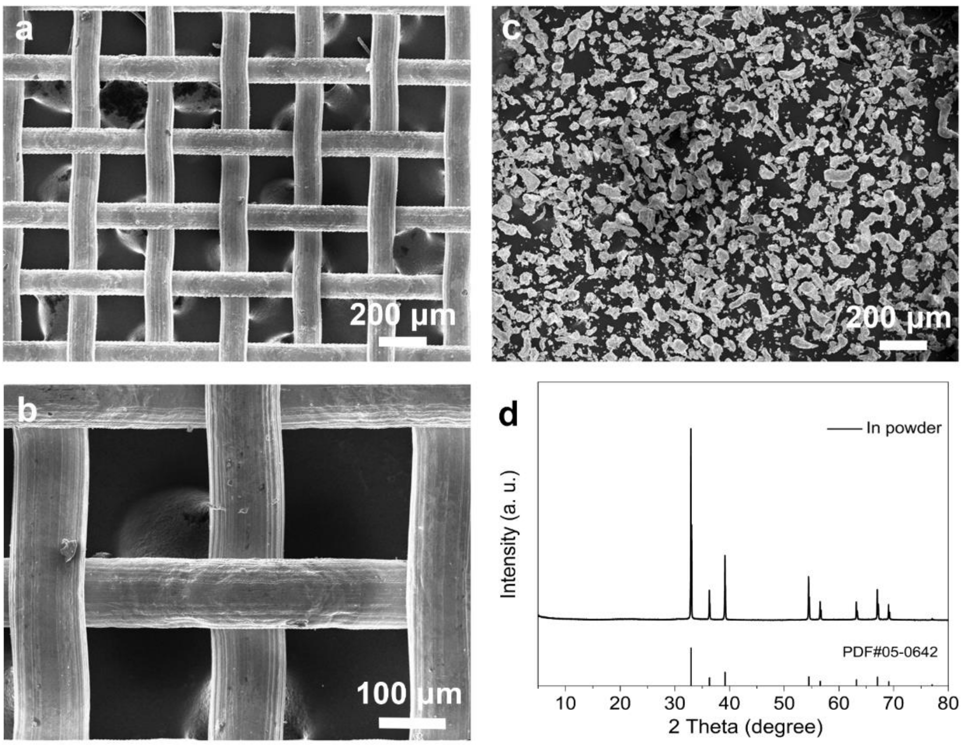

Fig. S1 SEM images of the **a, b** stainless steel meshes and **c** In powder. **d** XRD patterns of the In powder

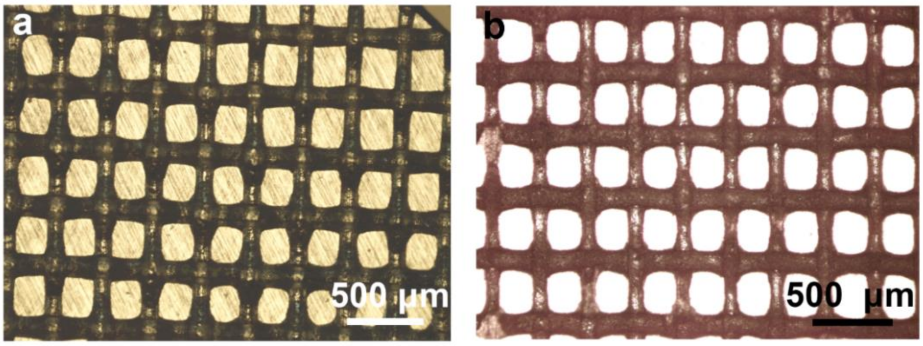

Fig. S2 Optical microscopic images of **a** the Zn electrodes after the rolling process and **b** the pristine ZnIn electrode

Fig. S3 Optical photographic image of the P-Zn electrode before and after In powder modification

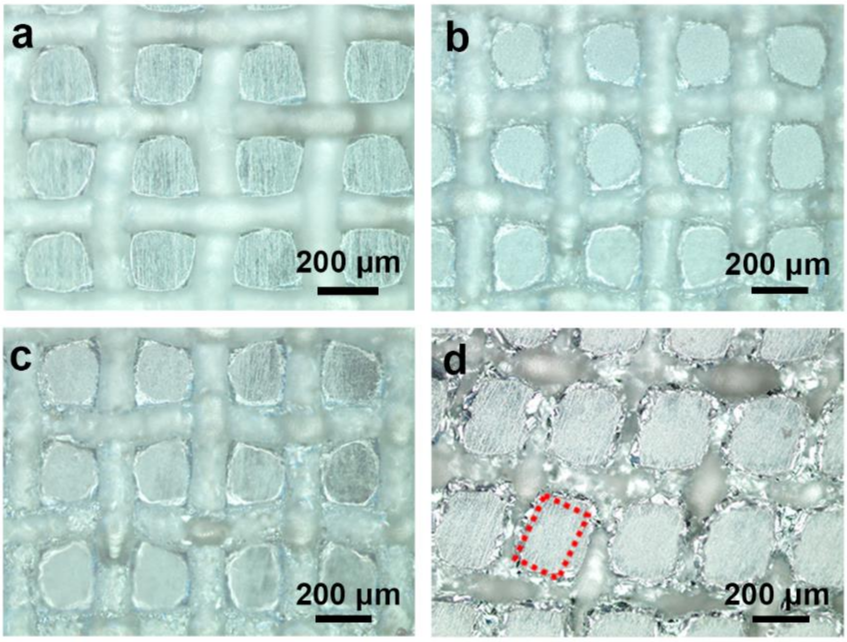

Fig. S4 Optical microscopic images of the Zn deposits on the ZnIn electrode with the areal capacities of **a** 0 mAh cm^{-2}, **b** 3.0 mAh cm^{-2}, **c** 5.0 mAh cm^{-2}, and **d** 10.0 mAh cm^{-2}

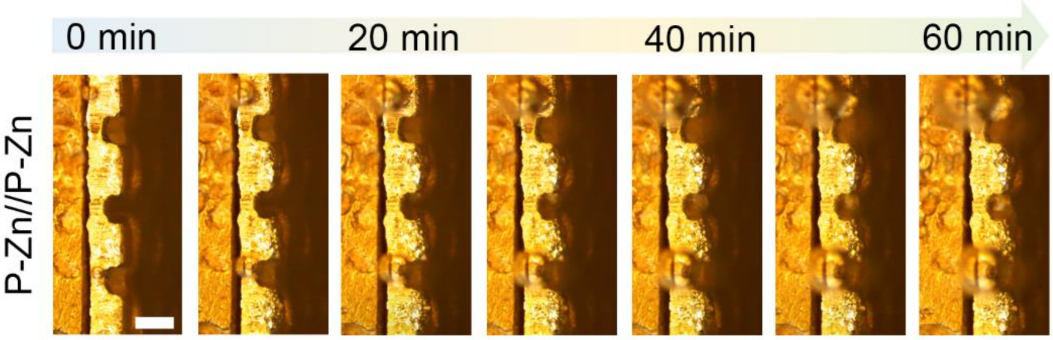

Fig. S5 In situ optical microscopic images of the Zn deposition on the P-Zn electrode. Scale bar: 100 μm

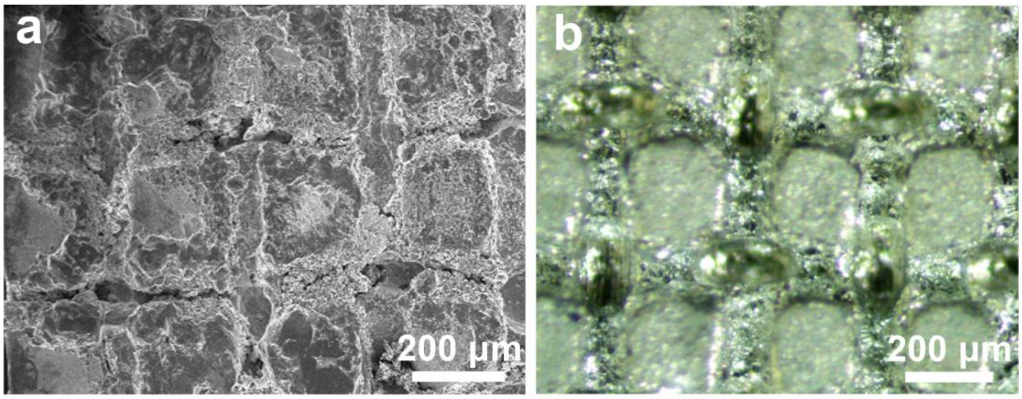

Fig. S6 a SEM image and **b** optical microscopic image of the Zn deposits on the ZnIn electrode with the areal capacities of 15.0 mAh cm^{-2}

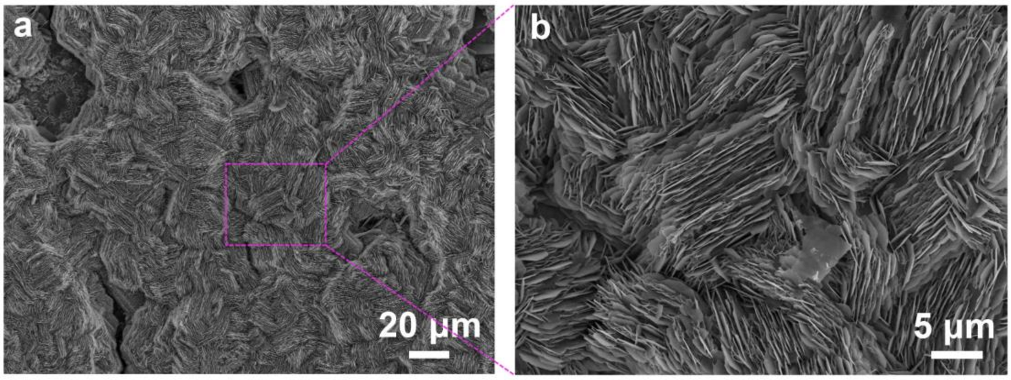

Fig. S7 SEM images of Zn deposits on the pristine Zn electrode with the current density of 1.0 mA cm^{-2} for 5 h

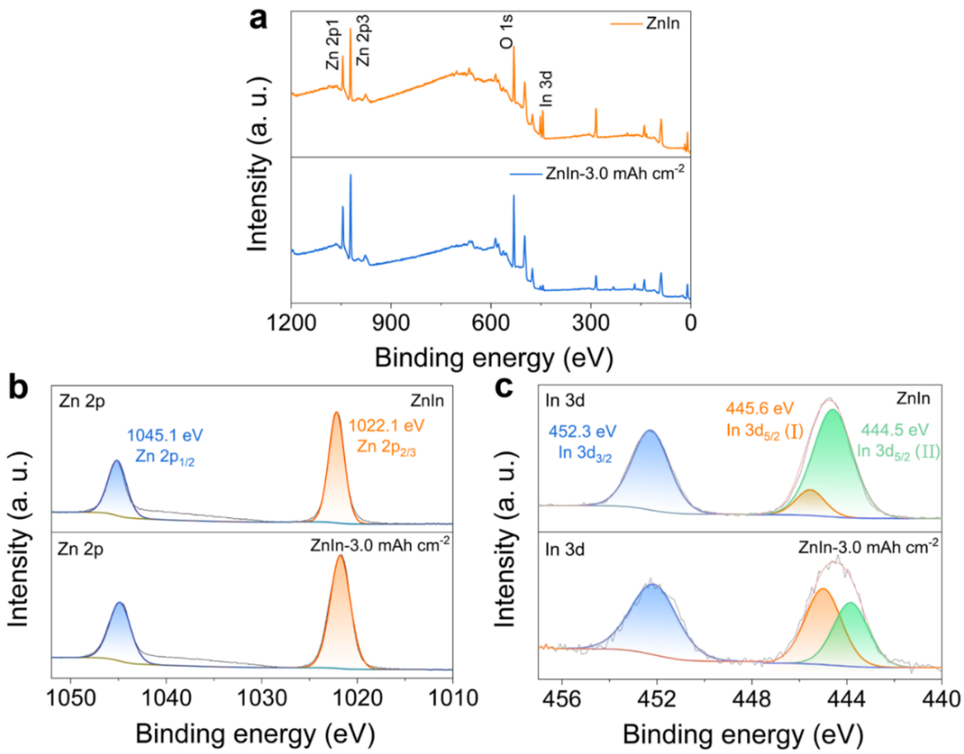

Fig. S8 a XPS full survey scan spectra and high-resolution core-level spectra of **b** Zn 2p and **c** In 3d for the pristine ZnIn electrode and the ZnIn electrode after Zn metal deposition

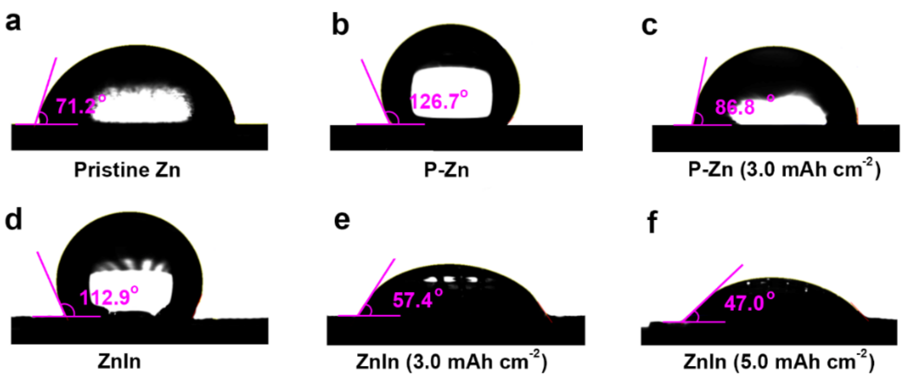

Fig. S9 Contact angles of the **a** pristine Zn, **b** P-Zn and **c** P-Zn electrode with the capacities of 3.0, and **d** pristine ZnIn electrodes and the ZnIn electrode with the capacities of **e** 3.0 and **f** 5.0 mAh cm^{-2}

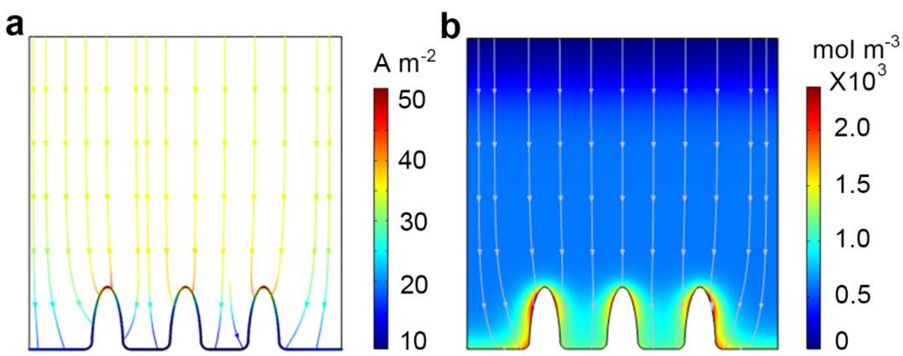

Fig. S10 Simulation results of **a** the current density and **b** the Zn ion concentration distribution on the pristine Zn electrode surface

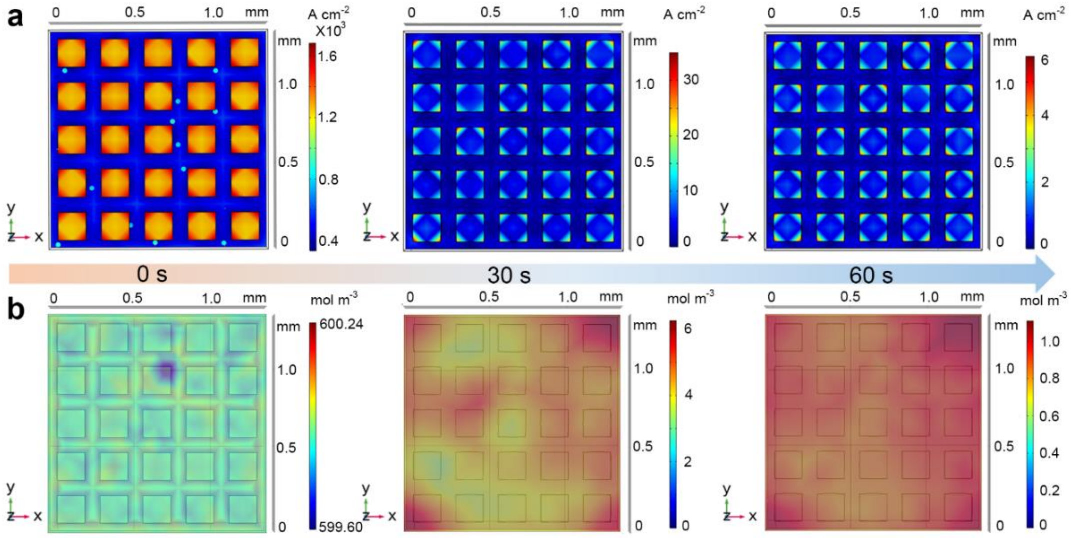

Fig. S11 2D view of the evolution process of **a-c** the current density and **d-f** the Zn ion concentration distribution on the ZnIn electrode surface

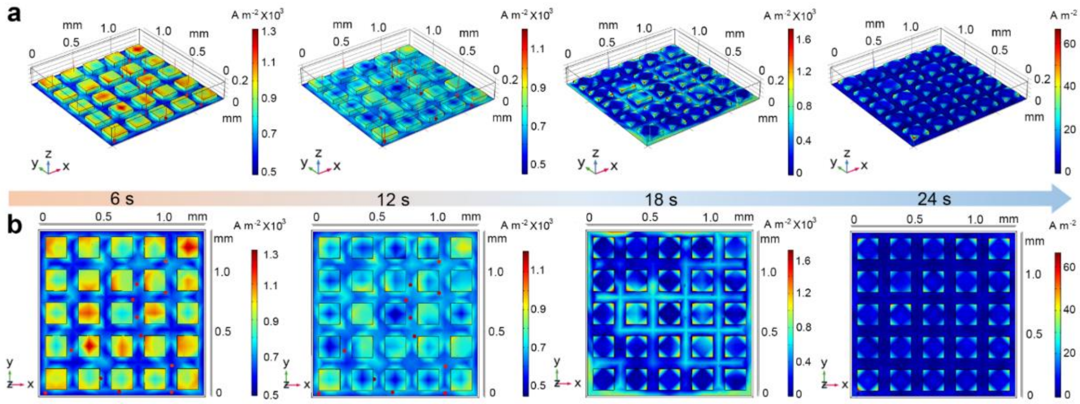

Fig. S12 a 3D view of the evolution process of the current density on the ZnIn electrode surface and **b** its corresponding 2D view

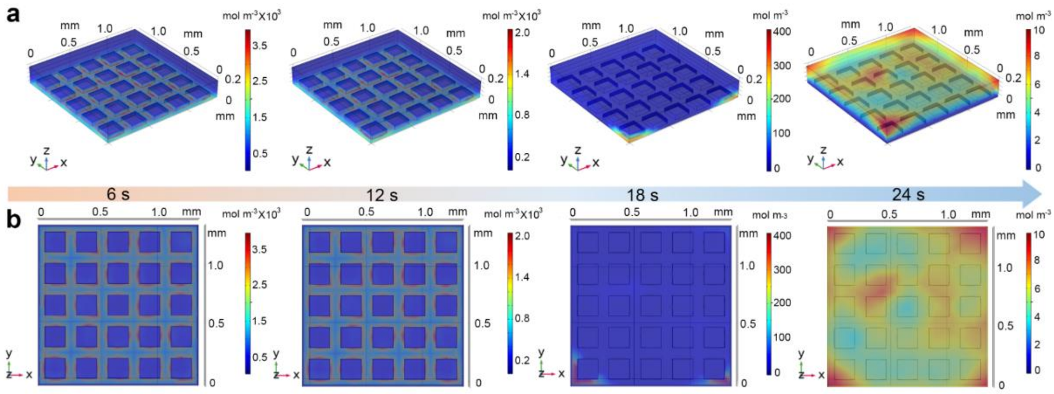

Fig. S13 a 3D view of the evolution process of the Zn ion concentration on the ZnIn electrode surface and **b** its corresponding 2D view

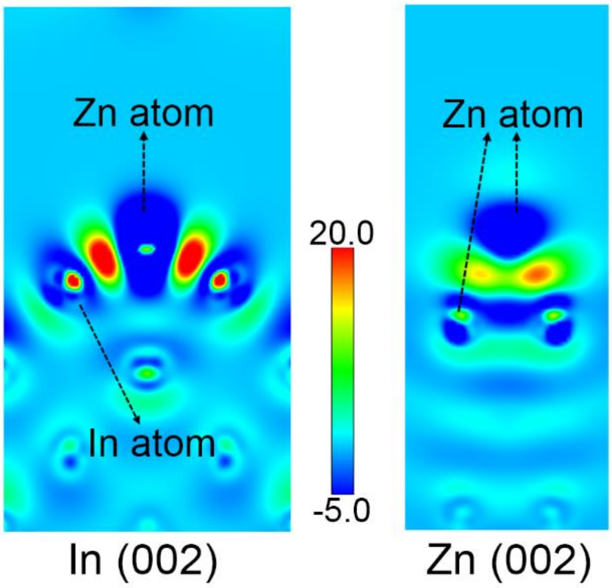

Fig. S14 Slice of the electron density difference map of the Zn atom on the In (002) and Zn (002) planes, respectively

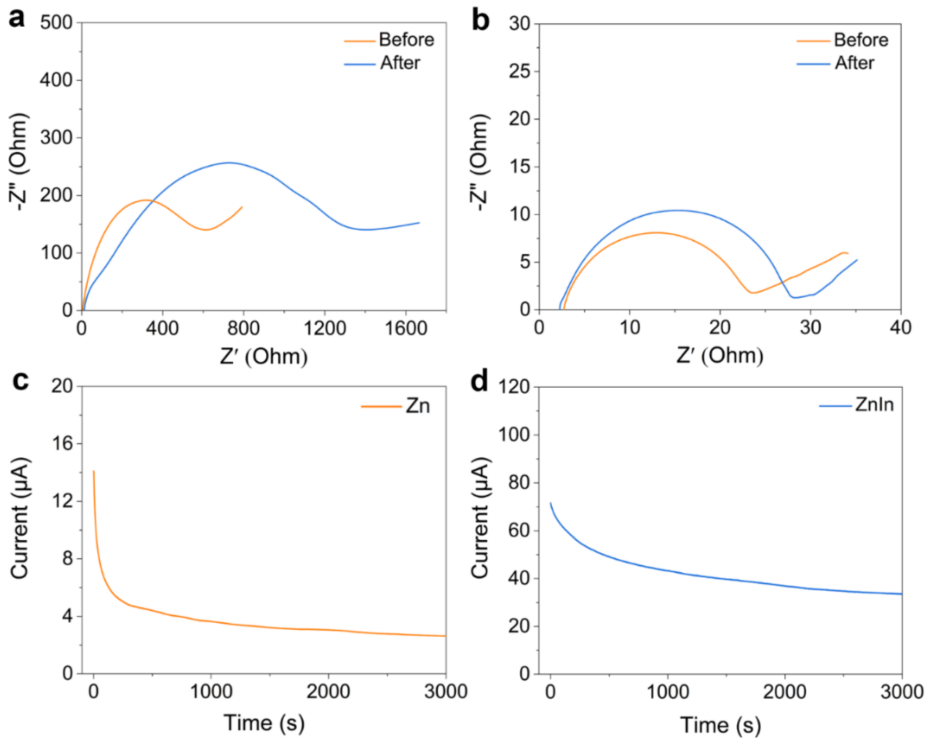

Fig. S15 Nyquist plots of the **a** Zn and **b** ZnIn symmetric batteries before and after polarization test and the corresponding current-time curves of the **c** Zn and **d** ZnIn symmetric cells under the constant voltage polarization of 5 mV.

The Zn ions transference number was obtained by the Evans' method [S1, S2]:

$$t_{Zn^{2+}} = \frac{I_S(\Delta V - I_0 R_0)}{I_0(\Delta V - I_S R_S)}$$

where I_0 and I_s are the currents of the initial and steady state, respectively and R_s and R_s represent the corresponding resistances, respectively. The ΔV means the applied voltage polarization.

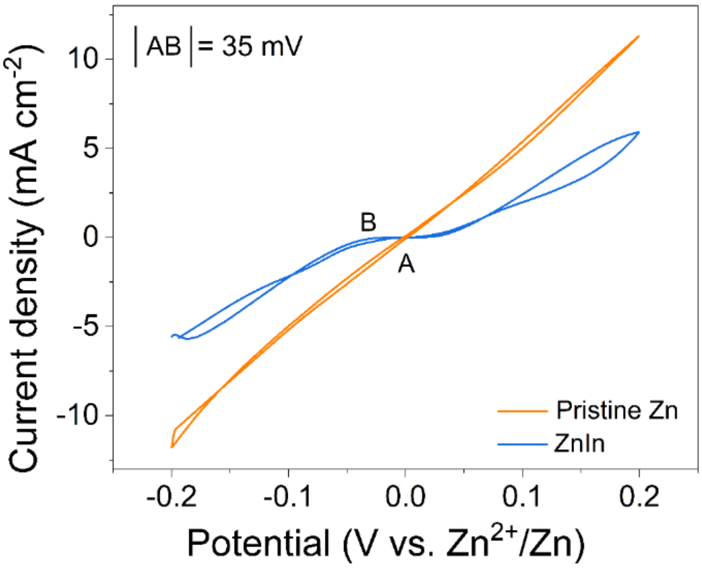

Fig. S16 CV curves of Zn plating/stripping on pristine Zn and ZnIn electrodes

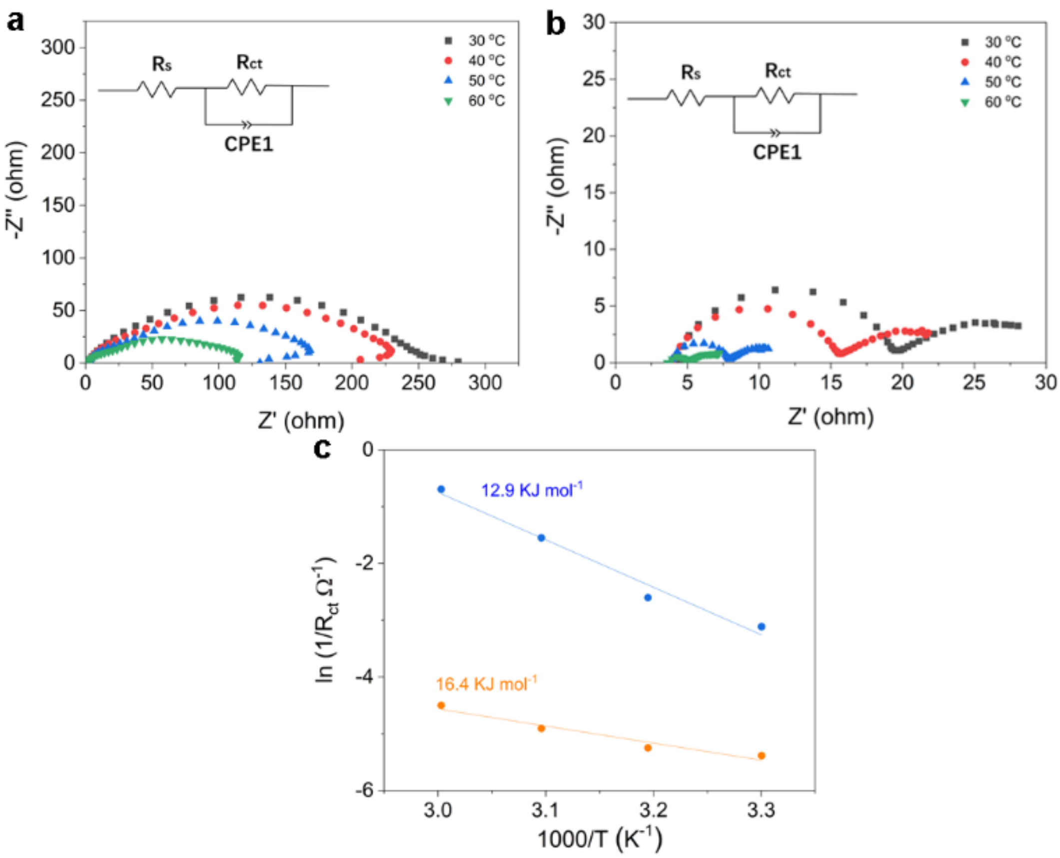

Fig. S17 The EIS curves of **a** pristine Zn and **b** ZnIn electrodes at different temperatures. **c** The corresponding desolvation activation energy values of the differnet electrodes

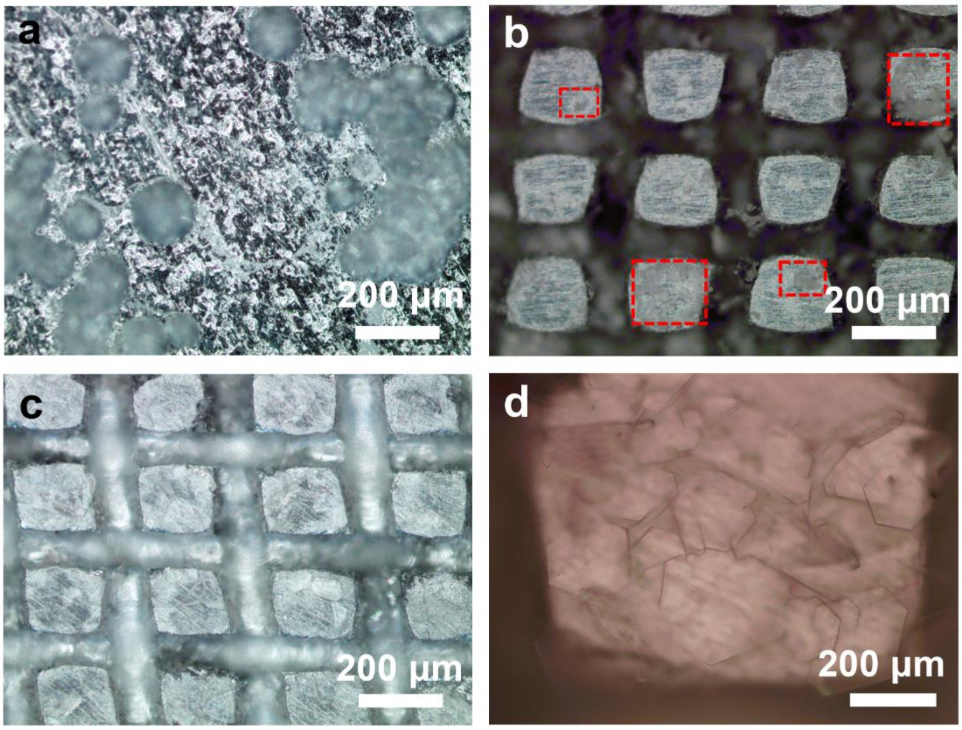

Fig. S18 Optical microscopic images of **a** pristine Zn and **b** P-Zn, and **c, d** ZnIn electrodes after cycling 100 h at the current density of 1.0 mA cm^{-2} with the area capacity of 1.0 mA cm^{-2}

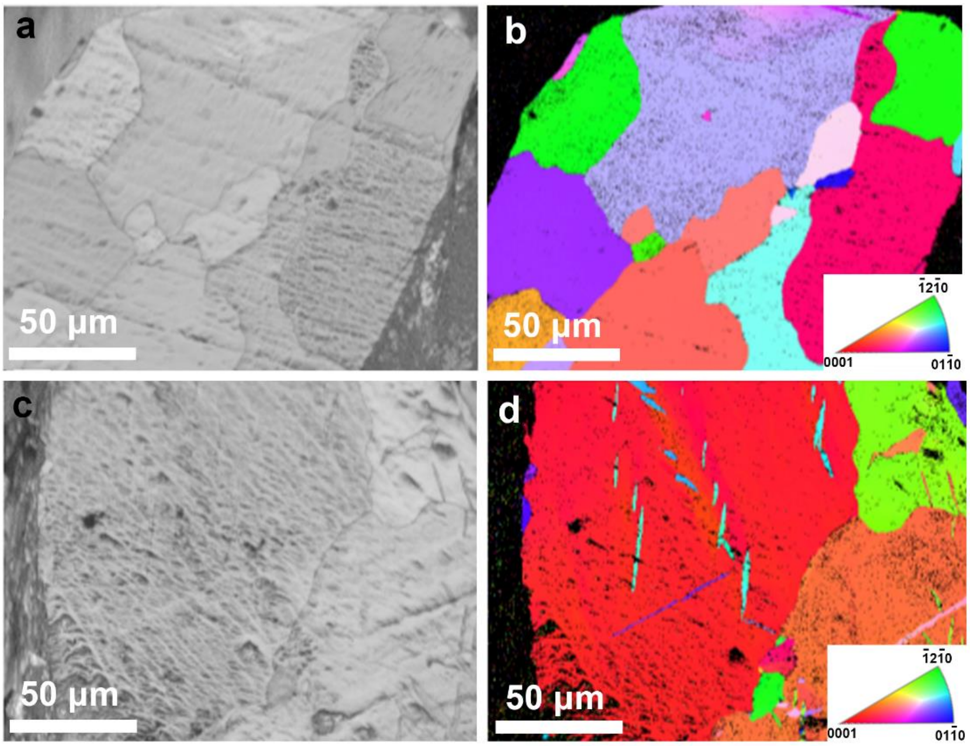

Fig. S19 Band contrast image and its corresponding EBSD mapping of the ZnIn electrode **a**, **b** before and **c**, **d** after cycling 100 h

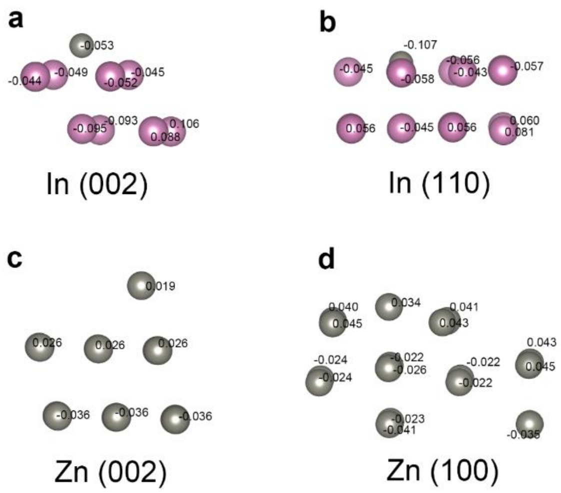

Fig. S20 Mulliken charge distributions of the Zn atom on the **a** In (002), **b** In (110), **c** Zn (002), and **d** Zn (100) planes

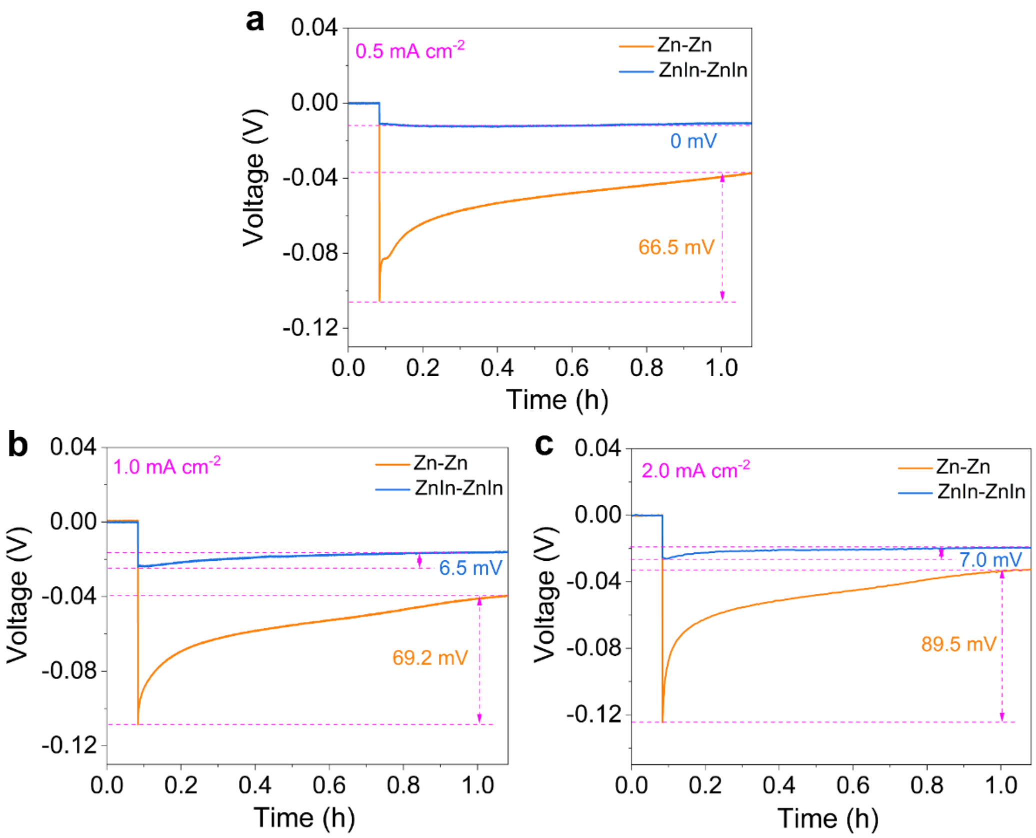

Fig. S21 Voltage profiles of Zn deposition on the pristine Zn and ZnIn electrodes at **a** 0.5 mA cm^{-2}, **b** 1.0 mA cm^{-2}, and **c** 2.0 mA cm^{-2}

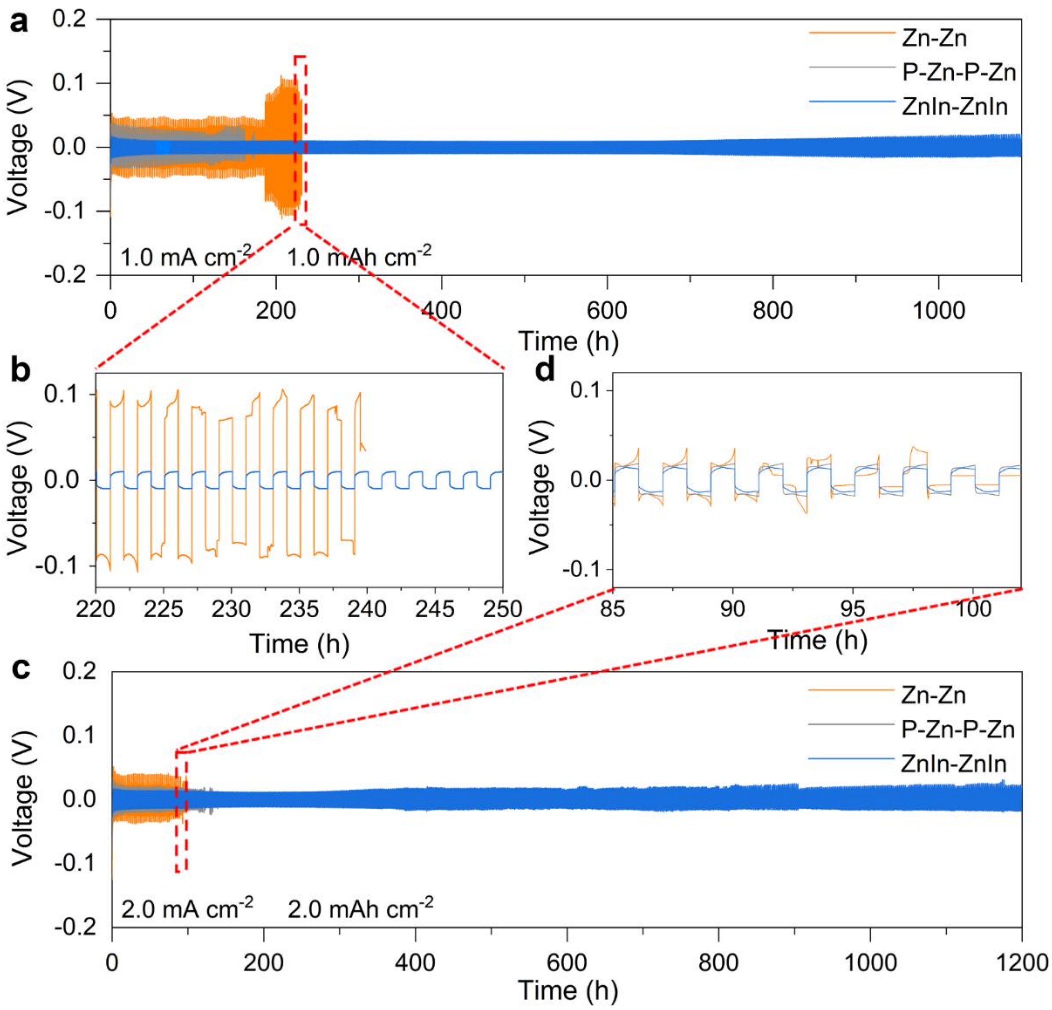

Fig. S22 Voltage profiles of pristine Zn, P-Zn, and ZnIn symmetric cells with plating/strapping conditions of **a** 1.0 mA cm^{-2} and 1.0 mAh cm^{-2} and **c** 2.0 mA cm^{-2} and 2.0 mAh cm^{-2}. **b, d** Their corresponding magnified curves at specific time in **a, c**

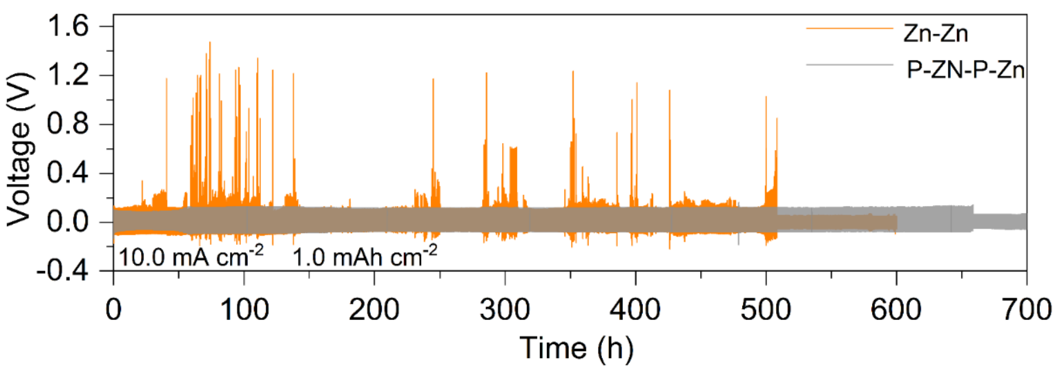

Fig. S23 Voltage profiles of the pristine Zn and P-Zn symmetric cells with plating/strapping conditions of 10.0 mA cm^{-2} and 1.0 mAh cm^{-2}

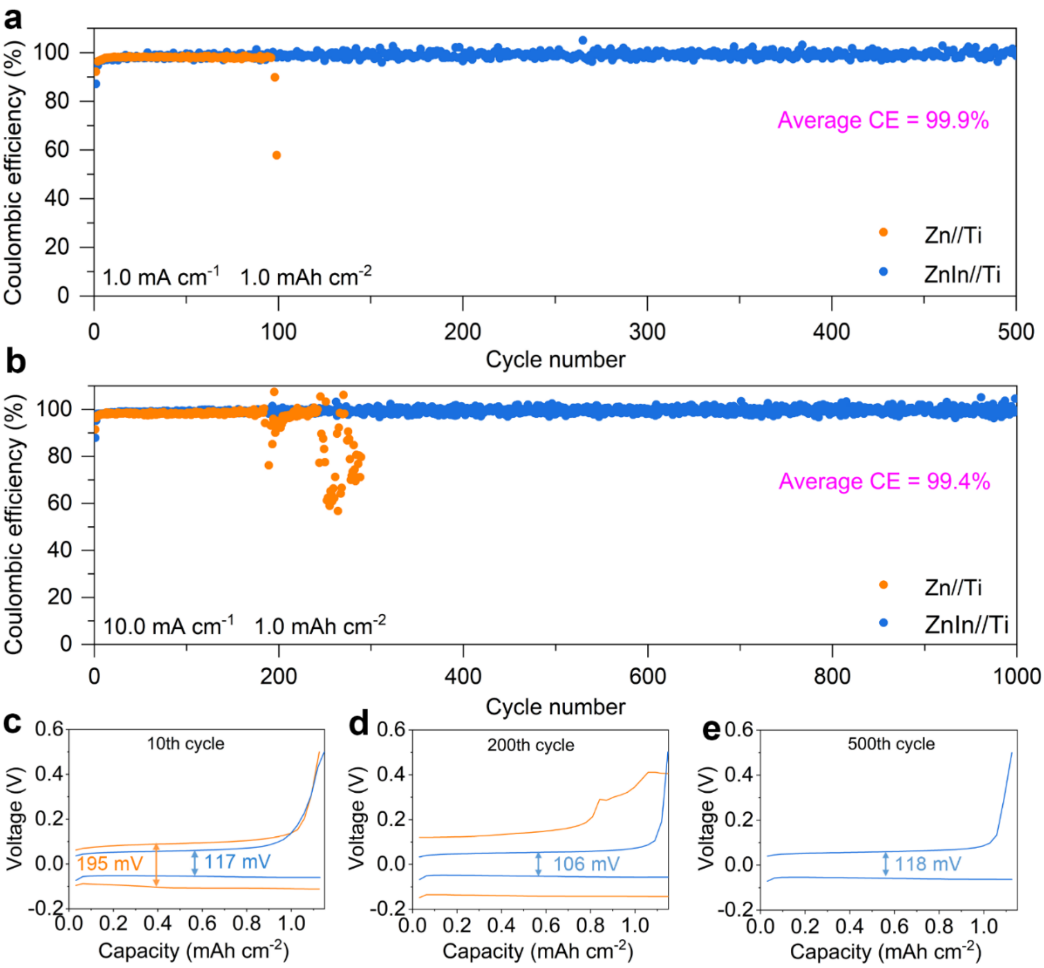

Fig. S24 Coulombic efficiency of the Zn plating/stripping on Ti foil at **a** 1.0 mA cm^{-2} and 1.0 mAh cm^{-2} and **b** 10.0 mA cm^{-2} and 1.0 mAh cm^{-2}. **c-e** Plating and stripping voltage profiles of Zn//Ti cell at 10.0 mA cm^{-2} and 1.0 mAh cm^{-2}

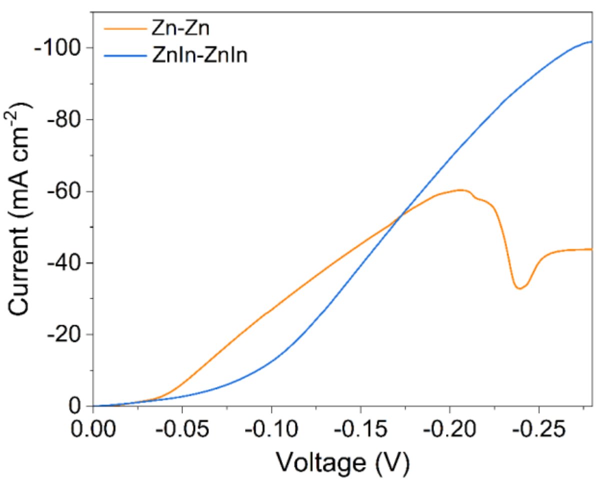

Fig. S25 Voltammetry of the pristine Zn and ZnIn symmetric cells at a scan rate of 1.0 mV s^{-1}

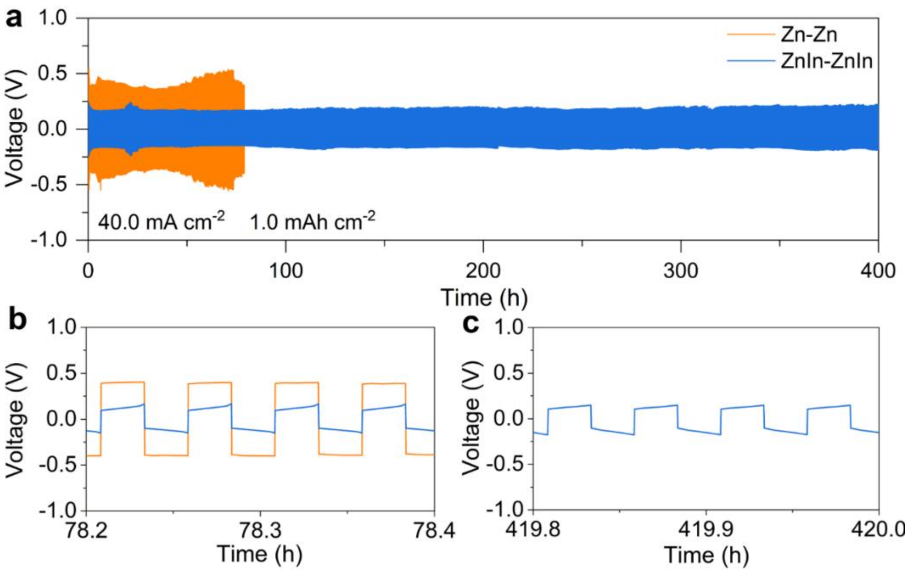

Fig. S26 a Voltage profiles of the pristine Zn and ZnIn symmetric cells with plating/strapping conditions of 40.0 mA cm^{-2} and 1.0 mAh cm^{-2} and **b, c** magnified voltage-time curves at different times

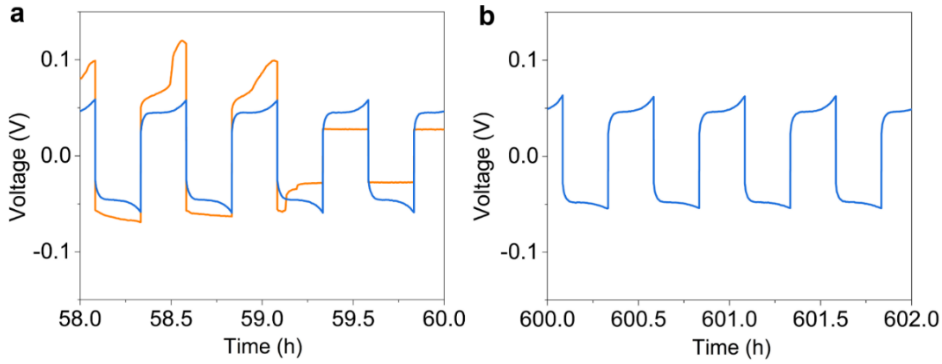

Fig. S27 Magnified voltage-time curves at different times in Fig. 4c

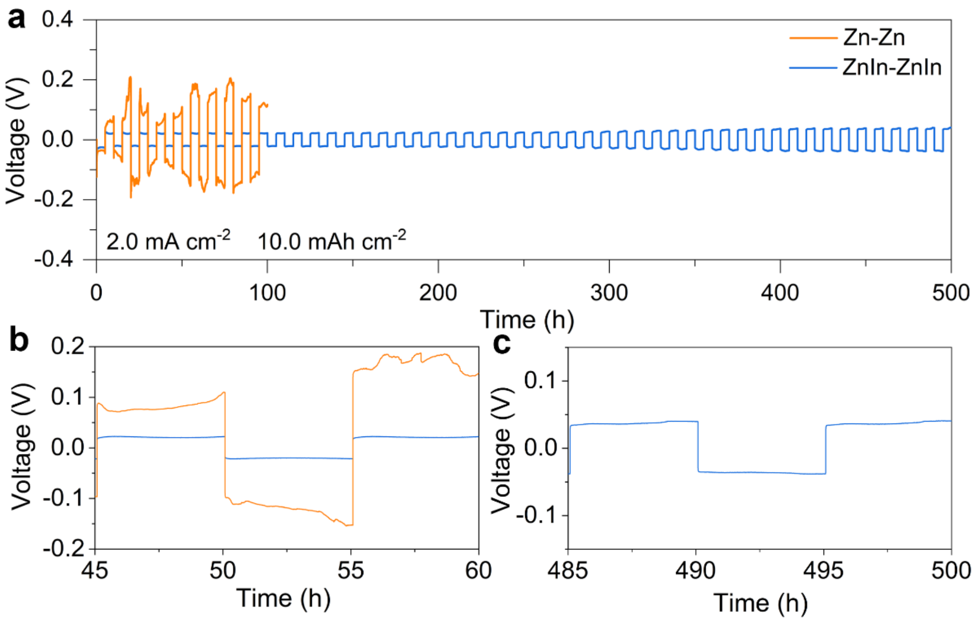

Fig. S28 a Voltage profiles of the pristine Zn and ZnIn symmetric cells with plating/strapping conditions of 2.0 mA cm^{-2} and 10.0 mAh cm^{-2} and **b, c** magnified voltage-time curves at different times

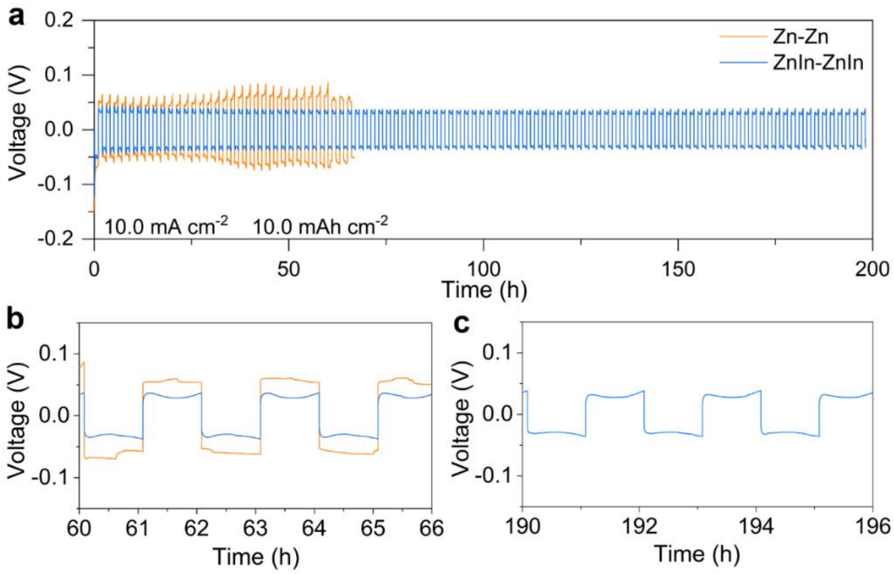

Fig. S29 a Voltage profiles of the pristine Zn and ZnIn symmetric cells with plating/strapping conditions of 10.0 mA cm^{-2} and 10.0 mAh cm^{-2} and **b, c** magnified voltage-time curves at different times

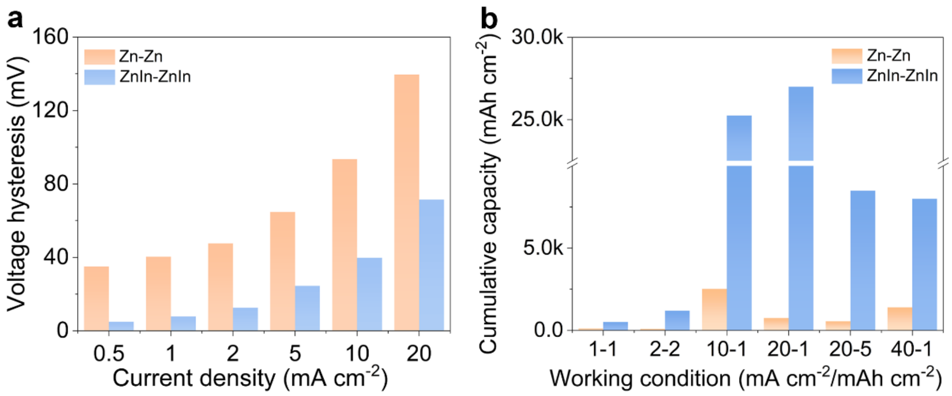

Fig. S30 Comparison of **a** the voltage polarization from rate performance and **b** the cumulative capacity of the pristine Zn and ZnIn symmetric cells at various working conditions

Table S1 Performance comparison of different modification strategies for Zn anode

Materials	Method/Mechanism	Current density (mA cm^{-2})	Areal capacity (mAh cm^{-2})	Time (h)	Refs.
Hydroxyl-rich silica ion sieve	Separator modification	1.0	1.0	3400	[S3]
		10.0	1.0	2550	
TiN	Protective coating layer	0.5	0.5	2800	[S4]
		1.0	1.0	2300	
		2.0	2.0	1050	
3D porous Ti	Nanoporous host	1.0	1.0	2000	[S5]
		10.0	0.5	500	
3D intertwined bacterial cellulose	In situ self-assembly	0.5	0.25	3000	[S6]
		5.0	2.5	570	
		5.0	5.0	300	
Zinc phosphate	Hydrothermal reaction	1.0	1.0	469	[S7]
		5.0	1.0	1976	
		10.0	1.0	500	
Sulfonate-rich	Ion-exchange layer	1.0	1.0	600	[S8]
		2.0	2.0	230	

Cross-linked gelatin	Artificial interface layer	1.0 2.0	1.0 2.0	4000 200	[S9]
Betaine	Electrolyte additive	0.5 2.0	0.5 2.0	4200 830	[S10]
Carbonyl-containing Layer	Ion redistributor and functional protective interphase	1.0 4.0 10.0	0.25 1.0 2.5	5000 2100 820	[S11]
ZnO/C nanoparticles	Host	10.0 20.0	1.0 1.0	400 150	[S12]
Bi	Termodynamics inertia and kinetics zincophilia	2.0 5.0 10.0 10.0	1.0 2.0 1.0 5.0	1700 1500 2000 310	[S13]
C/Cu nanocomposite decoration layer	Functional ultrathin separators	1.0 5.0 10.0	0.5 2.5 2.0	2000 650 600	[S14]
$Zn(NO_3)_2$ $6H_2O$ and $(NH_4)_2HPO_4$	Conversion coating	5.0 20.0	1.25 5.0	2000 470	[S15]
Graphdiyne	Atomic electrode	10.0 30.0	1.0 1.0	3200 250	[S16]
Metal-organic complex interphase	In situ complexing of metal-phytic acid	0.5 5.0	0.25 2.5	2000 1750	[S17]
Lanthanum nitrate	Electrolyte additive	1.0 10.0	1.0 5.93	1200 160	[S18]
Zn anode with 0.3 mAh cm^{-2} perdeposited layer	Stable zinc metal electrode surface morphologies	5.0 7.5 10.0	1.0 1.0 1.0	1000 700 500	[S19]
Poled ferroelectric coating layer	Deconcentrate and self-accelerate ion migration	1.0 10..0 20.0 40.0	1.0 2.0 2.0 2.0	4000 1250 625 225	[S20]
Hexamethylenetetramine	Electrolyte additive	5.0 5.0	1.0 5.0	4000 590	[S21]
Yolk-shell microspheres film	Artificial interface layer	1.0 10.0	0.5 1.0	3800 4000	[S22]
ZnIn anode	Surface patterning and zincphilic interface design	1.0 2.0 10.0 20.0 20.0 40.0	1.0 2.0 1.0 1.0 5.0 1.0	1020 1200 5050 2700 850 400	This work

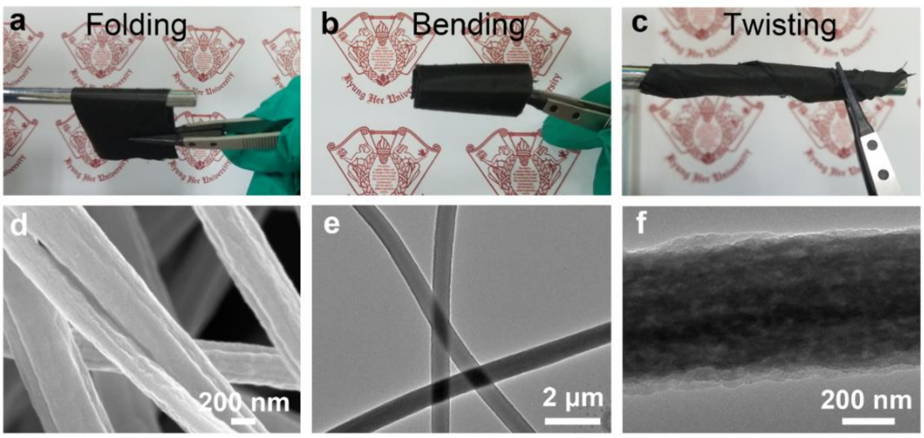

Fig. S31 Photographic images of the obtained CFs host at **a** folding, **b** bending, and **c** twisting states. **d** SEM and **e, f** TEM images of the CFs

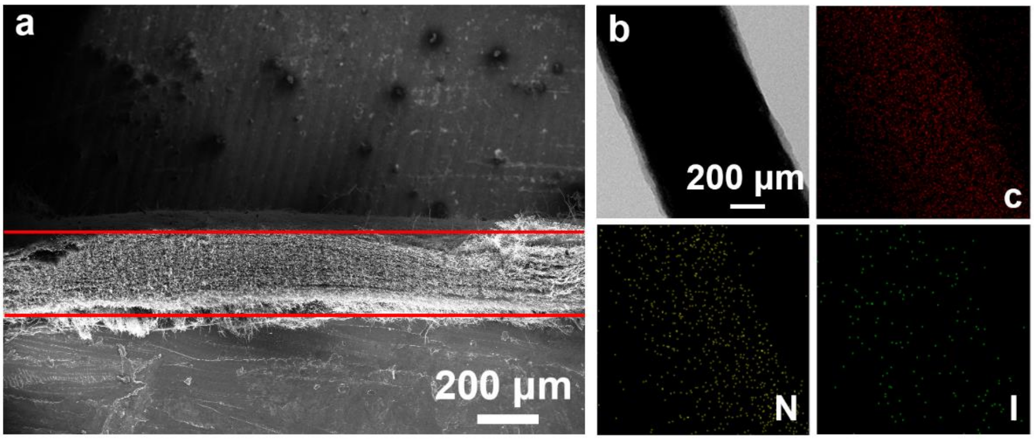

Fig. S32 a Cross-sectional SEM image of the CFs. **b** TEM image and the corresponding EDS mapping images of the I_2-CFs electrode

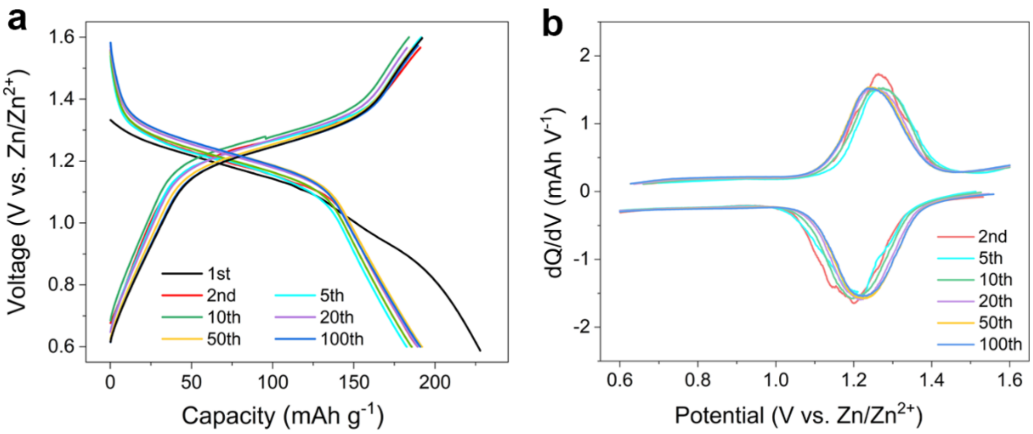

Fig. S33 a Charge/discharge profiles of the Zn//I_2-CFs full cell at the current density of 0.5 C and **b** their corresponding dQ/dV curves

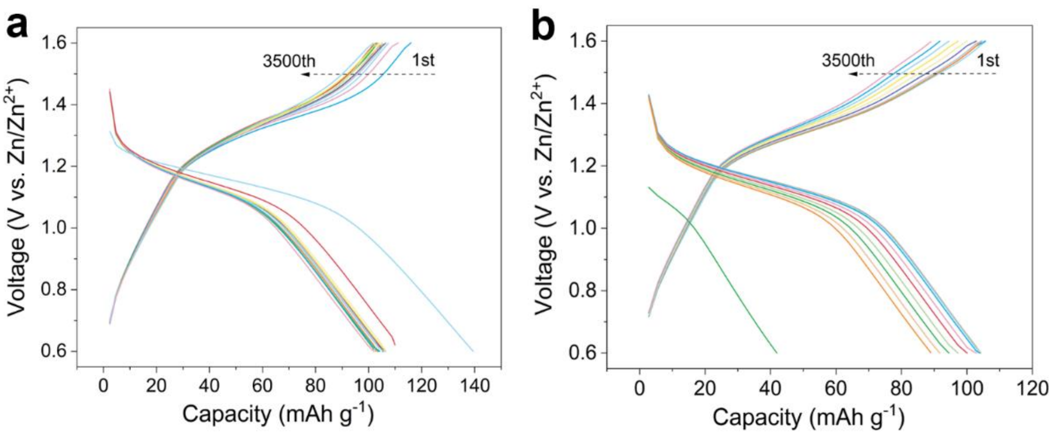

Fig. S34 Charge/discharge profiles of **a** the Zn//I_2-CFs and **b** ZnIn//I_2-CFs full cells at the current density of 5.0 C

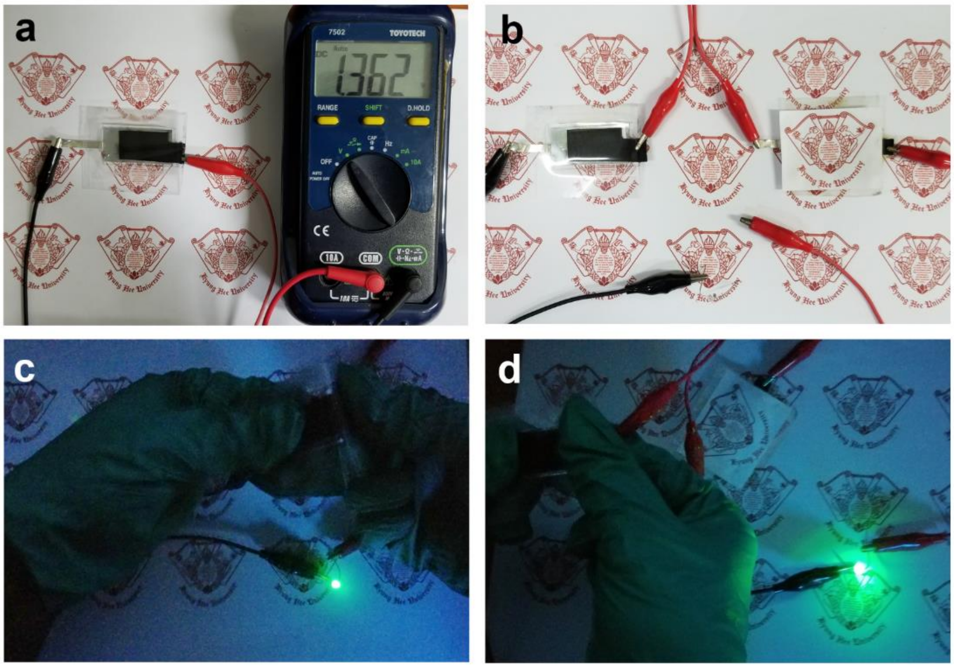

Fig. S35 **a** Open circuit voltage, **b** two cells connected in series, and **c, d** flexibility testing of the quasi-solid-state ZnIn//I_2-CFs pouch cell

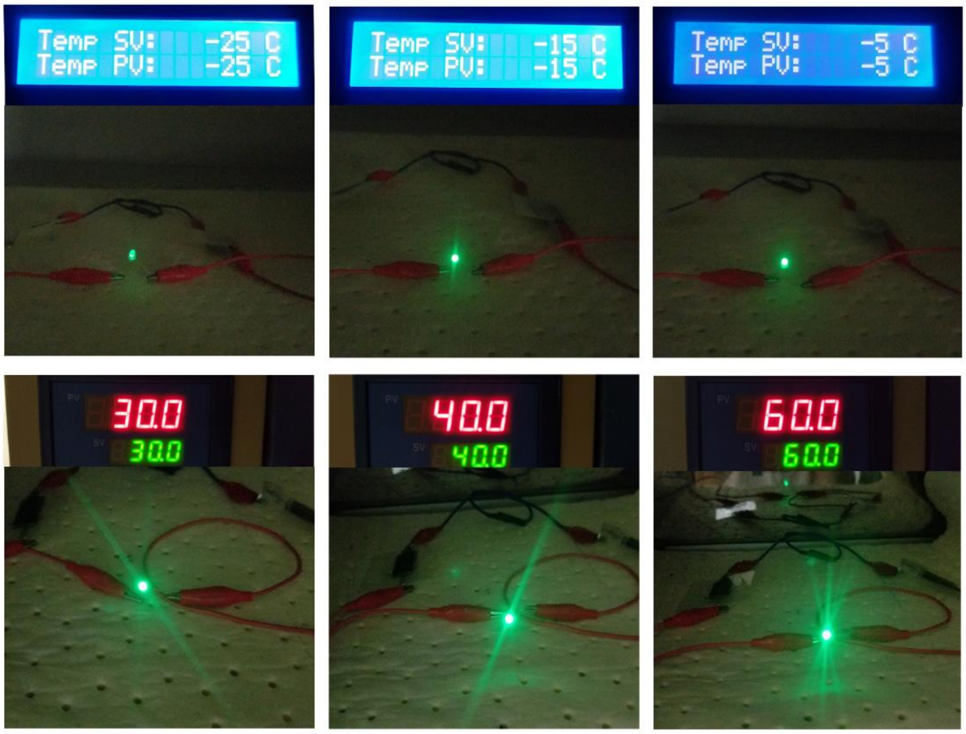

Fig. S36 Optical photographic images of the quasi-solid state ZnIn//I_2-CFs pouch cell powering a LED under different temperature conditions

Supplementary References

[S1] Evans, J., Vincent, C. A. & Bruce, P. G. Electrochemical measurement of transference numbers in polymer electrolytes. Polymer **28**, 2324-2328 (1987). https://doi.org/10.1016/0032-3861(87)90394-6

[S2] X. Yang, W. Li, Z. Chen, M. Tian, J. Peng et al., Synchronous dual electrolyte additive sustains Zn metal anode with 5600 h lifespan. Angew. Chem. Int. Ed. **135**, 202218454 (2023). https://doi.org/10.1002/ange.202218454

[S3] H. Gan, J. Wu, F. Zhang, R. Li, H. Liu, Uniform Zn^{2+} distribution and deposition regulated by ultrathin hydroxyl-rich silica ion sieve in zinc metal anodes. Energy Stor. Mater. **55**, 264-271 (2023). https://doi.org/10.1016/j.ensm.2022.11.044

[S4] J. Zheng, Z. Cao, F. Ming, H. Liang, Z. Qi et al., Preferred orientation of TiN coatings enables stable zinc anodes. ACS Energy Lett. **7**, 197-203 (2021). https://doi.org/10.1021/acsenergylett.1c02299

[S5] Y. An, Y. Tian, S. Xiong, J. Feng, Y. Qian, Scalable and controllable synthesis of interface-engineered nanoporous host for dendrite-free and high rate zinc metal batteries. ACS Nano 15, 11828-11842 (2021). https://doi.org/10.1021/acsnano.1c02928

[S6] S. Jiao, J. Fu, M. Wu, T. Hua, H. Hu, Tailoring Zn^{2+} desolvation kinetics and flux toward dendrite-free metallic zinc anodes. ACS Nano **16**, 1013-1024 (2021). https://doi.org/10.1021/acsnano.1c08638

[S7] S. Zhang, M. Ye, Y. Zhang, Y. Tang, X. Liu et al., Regulation of ionic distribution and desolvation activation energy enabled by in situ zinc phosphate protective layer toward highly reversible zinc metal anodes. Adv. Funct. Mater. **33**, 2208230 (2023). https://doi.org/10.1002/adfm.202208230

[S8] L. Zhang, J. Huang, H. Guo, L. Ge, Z. Tian et al., Tuning ion transport at the anode-electrolyte interface via a sulfonate-rich ion-exchange layer for durable zinc-iodine batteries. Adv. Energy Mater. **13**, 2203790 (2023). https://doi.org/10.1002/aenm.202203790

[S9] J. Shin, J. Lee, Y. Kim, Y. Park, M. Kim et al., Grain-directed zinc deposition in aqueous zinc ion batteries. Adv. Energy Mater. **11**, 2100676 (2021). https://doi.org/10.1002/aenm.202100676

[S10] H. Ren, S. Li, B. Wang, Y. Zhang, T. Wang et al., Molecular-crowding effect mimicking cold-resistant plants to stabilize the zinc anode with wider service temperature range. Adv. Mater. **35**, 2208237 (2023). https://doi.org/10.1002/adma.202208237

[S11] P. Wang, S. Liang, C. Chen, X. Xie, J. Chen et al., Spontaneous construction of nucleophilic carbonyl-containing interphase towards ultra-stable zinc metal anodes. Adv. Mater. **34**, 2202733 (2022). https://doi.org/10.1002/adma.202202733

[S12] P. Xue, C. Guo, L. Li, H. Li, D. Luo et al., A MOF-derivative decorated hierarchical porous host enabling ultrahigh rates and superior long-term cycling of dendrite-free Zn metal anodes. Adv. Mater. **34**, 2110047 (2022). https://doi.org/10.1002/adma.202110047

[S13] R. Zhao, X. Dong, P. Liang, H. Li, T. Zhang et al., Prioritizing hetero-metallic interfaces via thermodynamics inertia and kinetics zincophilia metrics for tough Zn-based aqueous batteries. Adv. Mater. **35**, 2209288 (2023). https://doi.org/10.1002/adma.202209288

[S14] Y. Li, X. Peng, X. Li, H. Duan, S. Xie et al., Functional ultrathin separators proactively stabilizing zinc anodes for zinc-based energy storage. Adv. Mater. **35**, 2300019 (2023). https://doi.org/10.1002/adma.202300019

[S15] Z. Xing, Y. Sun, X. Xie, Y. Tang, G. Xu et al., Zincophilic electrode interphase with appended proton reservoir ability stabilizes Zn metal anodes. Angew. Chem. Int. Ed. **135**, 202215324 (2023). https://doi.org/10.1002/anie.202215324

[S16] X. Luan, L. Qi, Z. Zheng, Y. Gao, Y. Xue et al., Step by step induced growth of zinc-metal interface on graphdiyne for aqueous zinc-ion batteries. Angew. Chem. Int. Ed. **62**, 202215968 (2023). https://doi.org/10.1002/anie.202215968

[S17] H. Liu, J. Wang, W. Hua, L. Ren, H. Sun et al., Navigating fast and uniform zinc deposition via a versatile metal-organic complex interphase. Energy Environ. Sci. **15**, 1872-1881 (2022). https://doi.org/10.1039/d2ee00209d

[S18] R. Zhao, H. Wang, H. Du, Y. Yang, Z. Gao et al., Lanthanum nitrate as aqueous electrolyte additive for favourable zinc metal electrodeposition. Nat. Commun. **13**, 3252 (2022). https://doi.org/10.1038/s41467-022-30939-8

[S19] Q. Li, A. Chen, D. Wang, Y. Zhao, X. Wang et al., Tailoring the metal electrode morphology via electrochemical protocol optimization for long-lasting aqueous zinc batteries. Nat. Commun. **13**, 3699 (2022). https://doi.org/10.1038/s41467-022-31461-7

[S20] P. Zou, R. Zhang, L. Yao, J. Qin, K. Kisslinger, et al., Ultrahigh-rate and long-life zinc-metal anodes enabled by self-accelerated cation migration. Adv. Energy Mater. **11**, 2100982 (2021). https://doi.org/10.1002/aenm.202100982

[S21] H. Yu, D. Chen, Q. Li, C. Yan, Z. Jiang et al., In situ construction of anode-molecule interface via lone-pair electrons in trace organic molecules additives to achieve stable zinc metal anodes. Adv. Energy Mater. **13**, 20300550 (2023). https://doi.org/10.1002/aenm.202300550

[S22] Q. Hu, J. Hou, Y. Liu, L. Li, Q. Ran et al., Modulating zinc metal reversibility by confined antifluctuator film for durable and dendrite-free zinc ion batteries. Adv. Mater. **35**, 2303336 (2023). https://doi.org/10.1002/adma.202303336